agriculture

MDPI

Article

Experimental Research on a Needle Roller-Type Electrostatic Separation Device for Separating Unginned Cotton and Residual Films

Yue Sun [1,2], Chunling Hu [1,2], Yangyang Li [1,2], Mingxiao Chen [1,2] and Ruoyu Zhang [1,2,*]

[1] School of Mechanical and Electrical Engineering, Shihezi University, Shihezi 832003, China
[2] Key Laboratory of Agricultural Equipment of Northwest China, Ministry of Agriculture and Rural Affairs, Shihezi 832003, China
* Correspondence: zryzju@gmail.com

Abstract: In the mechanized harvesting of cotton in Northwest China, problems result from the presence of a residual film, and it is difficult to remove the residual film in the cotton processing stage. In this study, a needle roller electrostatic separation device was designed for use with unginned cotton residual films, and a series of experiments was carried out. Through force analyses and charge testing of the seed cotton and the residual film, a theoretical basis was provided for separating them. Taking the residual film separation rate as the response index, the optimal parameter combination was determined with a response surface analysis of three factors and three levels, and a mathematical model was established. The test results showed that the optimal parameter set included a 25.3° corona electrode angle, a 172.3 mm corona electrode distance, and a 5.25 W discharge power. After optimization of the parameters for separation, the average residual film separation rate was 91.7%. This research provides data and technical support for the design of the machinery and the selection of the parameters used in treating machine-picked cotton and separating the residual film.

Keywords: machine picking; unginned cotton; residual film; electrostatic separation; response surface analysis

check for updates

Citation: Sun, Y.; Hu, C.; Li, Y.; Chen, M.; Zhang, R. Experimental Research on a Needle Roller-Type Electrostatic Separation Device for Separating Unginned Cotton and Residual Films. *Agriculture* **2023**, *13*, 324. https://doi.org/10.3390/agriculture13020324

Academic Editors: Jacopo Bacenetti and Jianping Hu

Received: 4 December 2022
Revised: 19 January 2023
Accepted: 25 January 2023
Published: 28 January 2023

Copyright: © 2023 by the authors. Licensee MDPI, Basel, Switzerland. This article is an open access article distributed under the terms and conditions of the Creative Commons Attribution (CC BY) license (https://creativecommons.org/licenses/by/4.0/).

1. Introduction

China's main cotton-growing regions are characterized by dry climates. Cotton planting involves film mulching and mechanized collection. Mechanized harvesting lacks selectivity, and this leaves mulch films mixed in the harvested cotton. During the processing of cotton and after the cleaning, ginning, and other processes, the mulch films are broken down into filaments and fragments. The amount of residue is increased exponentially, making it more difficult to remove. Spinning and weaving with lint containing film filaments and fragments reduce the spinning quality and cause serious financial losses to the processing enterprises [1–3].

Manual picking and mechanical and wind impurity removal are the main methods used for removing the residual films mixed with cotton [4–7]. In addition, machine vision-based recognition technologies [8–11], electrostatic adsorption separation, and so on have been developed in recent years. Among these methods, manual picking is labor-intensive and inefficient. Mechanical impurity removal involves multiple cleaning processes that may easily damage the cotton fibers, and the separation rate is low. Although machine vision recognition is effective, it is expensive and has stringent requirements that restrict large-scale applications. Electrostatic separation technology has been widely used in other industries due to its low energy consumption and high efficiency. [12,13] Zhang et al. [14] used Si and PET mixed particles as raw materials and used the difference in the electrical characteristics of the two materials for separation. Salama et al. [15] used a roller-type electrostatic separator to recover copper and aluminum from discarded wires, analyzed

a numerical model for the particle trajectories, and achieved good sorting results. In agriculture, electrostatic adsorption technology was used to recover residual film in the field. Xu et al. [16,17] discussed the effects of water content and voltage on the separation rate. This study provides theoretical support for recovering mulch films from the field. Qi et al. [18] developed an electrostatic recovery device for residual film and proved through testing that the device could separate the residual film from the soil. For the removal of residual film in machine-picked cotton processing, Guo et al. [19] proposed using the electrostatic adsorption method to remove impurities, but the conveyor belt structure of the device limited the efficiency for cotton processing and the winding of seed cotton and residual film was ignored, so there was still room to improve the method of impurity removal. Wang et al. [20] used the electrostatic adsorption method to remove residual film in stages but did not carry out in-depth research on the electrode arrangement and the operating parameters.

Most of the devices that use electrostatic adsorption in cotton picking machines to remove residual film have problems, such as a low degree of automation, dependence on manual operation, and a complex structure. In practice, it is difficult to adapt this method to factory conditions, and the cotton processing capacity per unit time is low. To overcome these limitations, a needle roller-type electrostatic separation device for unginned cotton and the residual film was designed in this study. The electrode position and operating parameters were flexible and adjustable to enable adaptation to different processing requirements. The combination of a corona electrode and a static electrode ensured that the electrostatic separation was enhanced when the electrostatic field strength was maximized. The earthing roller was continuously driven by the motor and continuously absorbed the residual film when working. The residual film adsorbed on the earthing roller was removed with negative pressure air to effect nonstop cleaning and keep the adsorption side of the earthing roller clean. All of the components work together to achieve stable and efficient separation and removal of the residual film. Additionally, the difference in the charge characteristics of the seed cotton and the residual film was studied. Single-factor and response surface optimizations were carried out for a needle-roller electrostatic separation device used to remove seed cotton residual film while focusing on the discharge power, corona pole distance, corona pole angle and other factors that may affect the efficiency of separating the seed cotton residual film, and the optimal parameter combination was obtained when the separation rate for the seed cotton residual film and the seed cotton residual film was highest. This work has enriched the application of electrostatic separation technology. The method can also be applied to the separations of residual films and plastic wraps in other agricultural products [21,22].

2. Device and Methods

2.1. Design and Construction of the Needle Roller-Type Unginned Residual Film Electrostatic Separation Device

Figure 1 illustrates the overall structure of the device. The device is composed of a frame, a motor, a negative pressure suction pipe, a corona electrode, and an electrostatic electrode, a grounding roller, and a dust exhaust fan. The grounding roller has an iron mesh structure, and the electrode on the test bench is a needle electrode (length: 1 m; distance between adjacent needle tips: 20 mm).

During operation, the grounding roller and the frame are grounded, and the corona electrode and the electrostatic electrode are connected to a negative high-voltage power supply. Because the curvature radii of the corona electrode tip and the grounding electrode rotating roller are very different, when a potential difference of more than 1.2~1.5 kV is applied between the two electrodes, the electric field intensity near the corona electrode will greatly exceed that near the grounding electrode. When the electric field exceeds the breakdown field strength of air, corona discharge occurs [23]. Then, air ionization occurs, and large numbers of positive and negative ions are generated, which move to the electrodes with opposite polarities to form a corona current. In the space outside the corona

zone, there are many space charges, i.e., negative ions and electrons. Under the action of the electric field, these ions move toward the ground electrode at a high speed. When they collide with the materials, they lose their speed and are attached to the materials; that is, the charged material enters the electric field [24,25]. The difference in electrical conductivity between the unginned cotton and residual film lies in the amount of charge, which results in different behaviors in the electric field. The conductive unginned cotton transfers electric charge to the grounding electrode very quickly, and its gravity force is far greater than the electric field force, so it falls into the unginned cotton recovery box due to the effect of gravity. The residual films with poor conductivity do not transfer charge or transfer it very slowly, so they are adsorbed by the ground electrode, rotate with the roller, and are then removed by the film removal device. The structure design of this device is shown in Figure 2.

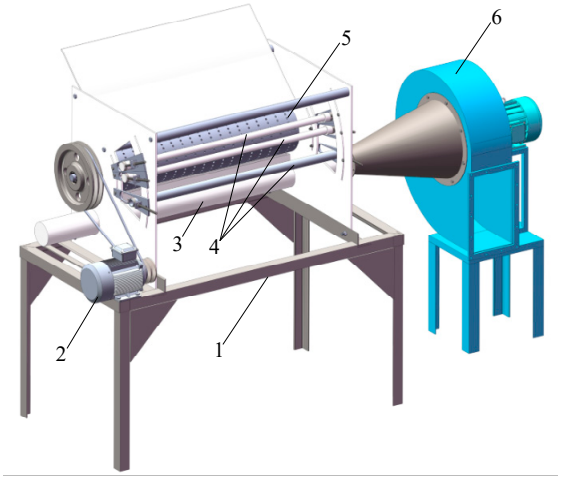


Figure 1. Schematic diagram of the needle roller-type residual film electrostatic separation device. 1. Frame; 2. Motor; 3. Negative pressure suction pipe; 4. Corona electrode and electrostatic electrode; 5. Grounding roller; 6. Dust exhaust fan.

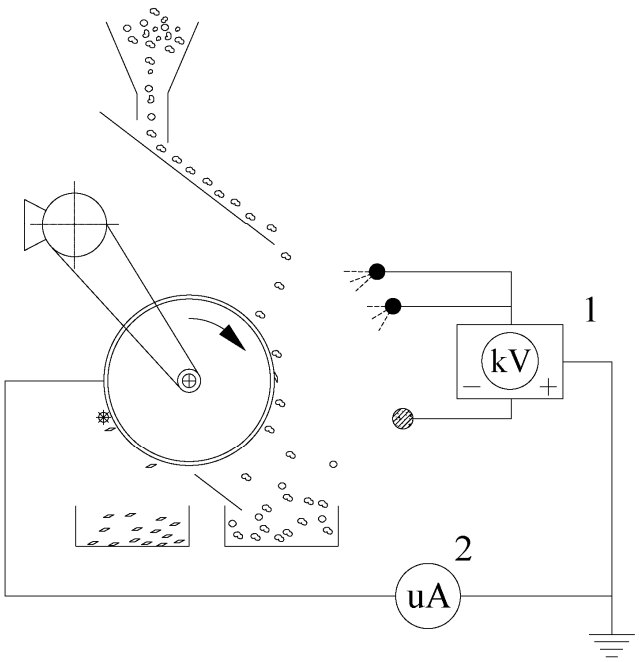


Figure 2. Structure design drawing of the needle roller-type electrostatic separator: 1. Electrostatic generator (Electrostatic voltmeter) and 2. Microampere ammeter.

The electrode arrangement is shown in Figure 3. The angle between the corona pole and the center axis plane of the ground roller is θ_1, the distance between the corona pole and ground roller surface is S_1, the angle between the static electrode and the center axis plane of the ground roller is θ_2, and the distance between its surface and the surface of the ground roller is S_2.

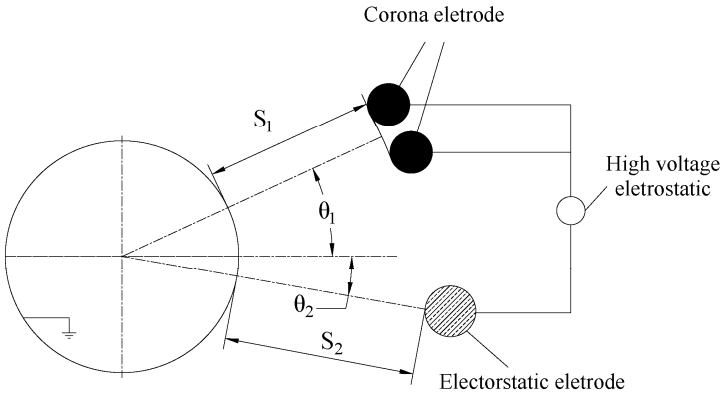


Figure 3. Schematic diagram of the electrode positions.

2.2. Material Charge Tests

To explore the conductance of the seed cotton and the residual film and the material charge moving through the ionized environment in free-falling motion, a material charge test was carried out.

Forty kilograms of Tianyun No. 0769 unginned cotton, with a moisture range of 6.5–9.0%, was utilized in this experiment. First, five kilograms of unginned cotton was randomly selected, and the residual films were picked out manually. Then, 6 samples (6–12 g for each) were selected for testing. A few pieces of the residual film were picked up from the field, and 6 pieces of the residual film with masses of 0.04–0.06 g and areas of 0.0045–0.0055 m^2 were selected as the test samples. The test temperature was 26.7–28 °C, and the humidity was 30–40%.

The main devices included a needle-roller-type residual film electrostatic separation device independently constructed by the research team and a digital charge meter (HEST-111A, Beijing Huace Testing Instrument Co., Ltd., Beijing, China). The measurement range was 0.1 pC–200 nC, and the accuracy was ±0.5%. The operating temperatures were −10–45 °C, with 80% relative humidity (RH). Additional instruments used in this study included a digital high-voltage meter (EST105A, Beijing Huajinghui Technology Co., Ltd., Beijing, China), a high-voltage electrostatic generator (HC-JDGC-C, Yangzhou Huachun Electrostatic Engineering Co., Ltd., Yangzhou, China), and an electronic scale (XK3190-A7, Shanghai Dachuan Weighing Apparatus Co., Ltd., Shanghai, China.

To better understand the electrostatic separation mechanism, the charging performance of the residual film was tested. The residual film corona electrification measurement device consisted of a DC high-voltage electrostatic generator, electrodes, and a digital charge meter (including a Faraday cylinder). The test steps were as follows: the test sample was completely discharged first. Then, the sample was put into the operating high-voltage electrostatic separator, and the charged material in the lower Faraday cylinder was received. After that, unginned cotton was placed on an insulating board to suspend it in a high-voltage electrostatic environment for 120 s to ensure that the material would fall naturally during the instantaneous charge test [26,27]. The material charge test device is shown in Figure 4.

The saturation charge of the material was defined as follows: in the negative corona discharge under a steady state, the charge accumulated on the surface of the material no longer changes with time. The instantaneous charge was defined as follows: in the negative corona discharge at a steady state, the material falls naturally.

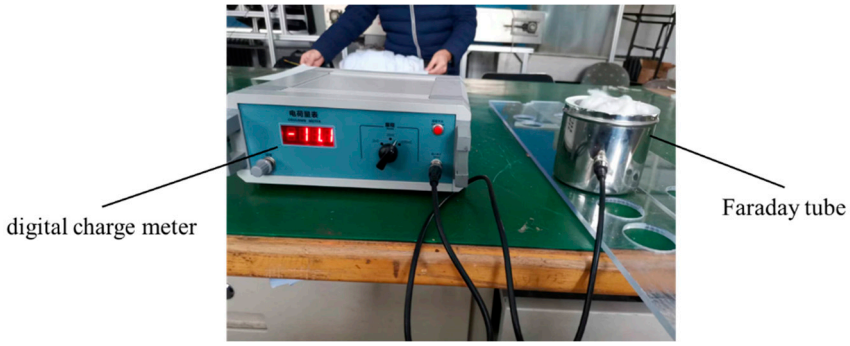


Figure 4. Material charge test device.

2.3. Test Method for Separation of the Residual Film from Unginned Cotton

According to the research described in Section 3.3.1, the main factors affecting the separation of the residual film were the corona electrode angle θ_1, corona electrode distance S_1, electrostatic electrode angle θ_2, and distance S_2, discharge power, and so on. Based on these factors, single-factor tests were carried out under the same conditions to investigate the influence of each factor on the separation of the residual film.

Based on the three significant factors that affected the separation rates determined in the single-factor experiments, the Box-Behnken design principle of the response surface analysis method was used [28–30], and the corona electrode angle *A* and the corona electrode distance *B* were determined. The values of the factors and levels for the discharge power *C* and the residual membrane separation rate *Y* were used as the response values for evaluation, and a three-factor and three-level test scheme was designed. The factor and level coding are shown in Table 1.

Table 1. Factor and level coding of the response surface analysis.

Factor	Level		
	−1	**0**	**1**
Corona electrode angle A/°	15	25	35
Corona electrode distance B/mm	142.5	177.5	212.5
Discharge power C/w	3.75	4.5	5.25

A total of 1000 g of unginned cotton and 10 pieces of residual films (the masses were 0.04~0.06 g, and the areas were 0.0045~0.0055 m^2) were evenly mixed, and a separation test was conducted using the needle roller-type electrostatic separation device to measure the separation rate. The test was repeated 6 times, and the average value was taken as the test result.

The separation rate (Y) was defined as the ratio of the number of pieces of residual film separated to the number of pieces of the residual film mixed into the unginned cotton before the test.

$$Y = \frac{n}{N} \times 100\%$$

where Y is the separation rate, %; n is the number of residual film pieces separated; and N is the number of residual film pieces mixed into the unginned cotton before the test.

3. Results and Discussion

3.1. Force Analyses of Charged Materials

The materials are equivalent to spherical particles, and both gravitational force F_g and centrifugal force F_c act on all particles. [14,22,25] The stress analysis and motion trajectory of unginned cotton and residual film after charging were shown in Figure 5.

$$F_g = mg \quad (1)$$

where m is the mass of the material [g], and g is the acceleration of gravity (g = 9.8 m s^{-2}).

$$F_c = \frac{mv^2}{R} \tag{2}$$

where v is the particle speed [ms^{-1}], and R is the roll electrode radius [m].

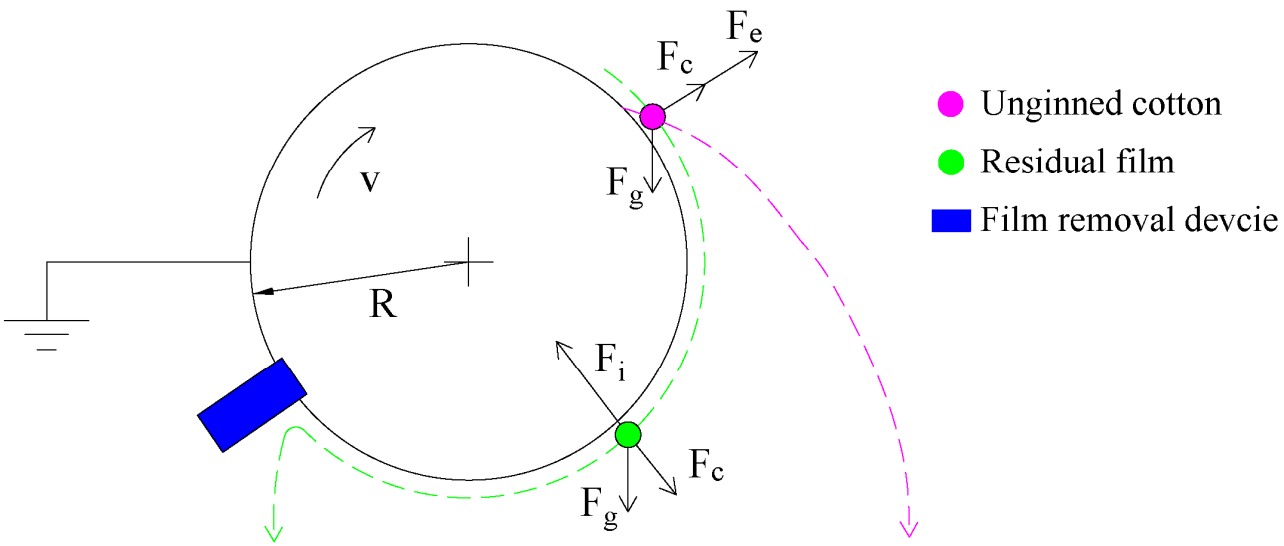


Figure 5. Schematic diagram showing the material forces and motion trajectory.

The electric image force F_i acting on the material was calculated as follows:

$$F_i = \frac{Q^2}{4\pi\varepsilon_0 r^2} \tag{3}$$

where Q is the charge gained by the particle, ε_0 is the vacuum permittivity and r is the radius of a particle. This force tends to pin the residual film to the ground roller. Residual films are not affected by electrostatic induction created by the electrostatic electrode. Therefore, the coulomb force on the residual film can be ignored. The gravitational component of the residual film perpendicular to the surface of the grounded roller electrode and its combined force of centrifugal force is not enough to break the bond of the electrical image force F_i, the force of the material satisfies Formula (4). So it adheres to the ground roller electrode under the leading role of F_i, and for finally stripped by the film removal device.

$$F_i > F_c + F_{gn} \tag{4}$$

where F_{gn} is the component of the gravitational force normal to the surface of the grounded roller electrode.

The Coulomb force F_e on the material was calculated as follows:

$$F_e = QE \tag{5}$$

where E is the electric field generated by the static electrode [V m^{-1}].

Conductive unginned cotton rapidly loses charge by conducting the charge acquired in the corona discharge region to the ground roller electrode, at which point the electric image force on the seed cotton is negligible. Then, by electrostatic induction, it acquires a charge for which the sign is opposite to the polarity of the high voltage potential (Study Results 3.2). It is affected by three forces, i.e., the Coulomb force F_e, the gravity force F_g and the centrifugal force F_c, the force of the material satisfies Formula (6). It disconnects from the roller under the leading action of the coulomb force and the centrifugal force, and then moves in a parabolic path.

$$F_{gn} < F_e + F_c \tag{6}$$

3.2. Results and Analyses of the Charge Tests performed on the Seed Cotton and Residual Film

After measuring the amount of charge on the residual film, it was found that the charge accumulated by the residual film in the negative corona environment was negative (Table 2). Due to the insulating properties of the residual film itself, the accumulated charge was not easily lost. The average charge was approximately −37.81 nC, the instantaneous charge was maintained at −32.91 nC, and the instantaneous charge rate reached 87%. Therefore, the residual film was rapidly charged in an ionized environment, and it can be proven that the residual film quickly obtains the charge of the ionized environment during free fall.

Table 2. Unginned cotton and residual film charge test results.

	Unginned Cotton				Residual Film		
	Sample NO.	**Instantaneous Charge (nC)**	**Loss of Charge State (nC)**	**Saturated Charge (nC)**	**Sample Area (mm^2)**	**Instantaneous Charge (nC)**	**Saturated Charge (nC)**
	1	−3.97	1.17	−8.33	0.0045	−28.73	−31.73
	2	−3.77	1.10	−6.63	0.0050	−34.80	−36.93
	3	−3.27	1.03	−4.60	0.0045	−27.73	−42.47
	4	−3.07	1.10	−7.13	0.0050	−34.27	−36.67
	5	−4.00	1.33	−6.63	0.0055	−37.47	−40.57
	6	−3.17	1.33	−9.43	0.0050	−34.50	−38.53
Mean value		−3.54	1.18	−7.13		−32.91	−37.81

The electric charge of the unginned cotton was measured. The results (Table 2) showed that the electric charge obtained by the unginned cotton in the negative corona environment was still negative. The electricity (instantaneous charge) was −3.54 nC. When some of the unginned cotton was in contact with the ground electrode, the charge carried by the unginned cotton was positive because the moist cotton fiber acted as a conductor, and its own negative charge dissipated faster. When the charge flowed into the ground, and due to the influence of the inductive charge of the electrostatic electrode, the positive charge played a leading role. At this time, the surface of the unginned cotton was positively charged, and the average amount of charge carried was 1.18 nC.

Analyses of the charging characteristics of the unginned cotton and the residual film showed that the uncharged materials were charged instantly when they passed through the ionization environment. Due to the characteristics of the unginned cotton and residual film, the charging processes were very different (Figure 6). The air around the corona electrode was ionized, the ions flowed to the grounding roller, and all of the particles were negatively charged by ion bombardment when passing through the ionization space. The residual film went through two states, namely, charge and adsorption (stable). The state of the unginned cotton included two cases: charged-no contact with the ground roller-free falling and charge-contacting with the ground roller (lose charge)-continual falling. In this process, the electrostatic electrode repelled the negatively charged particles and further increased the electric field force of the material. This improved the separation, which was consistent with the results of a previous study [22].

3.3. Test Results and Analyses for Separation of the Residual Film from the Unginned Cotton

3.3.1. Effect of Electrode Position and Operating Parameters on the Separation Rate

With a discharge power of 1.5 W, a corona electrode distance of 177.5 mm, a θ_2 of 10°, and an S_2 of 180 mm, separation experiments were carried out with different corona electrode angles. The curve in Figure 7a depicts the relationship between the corona electrode angle and the residual film separation rate. The results indicated that an increase in the corona electrode angle improved the separation rate, but when it exceeded 25°, the separation rate decreased, so the optimum angle for the corona electrode was between 15° and 35°. A correlation analysis was carried out with corona electrode angles of 0–35°.

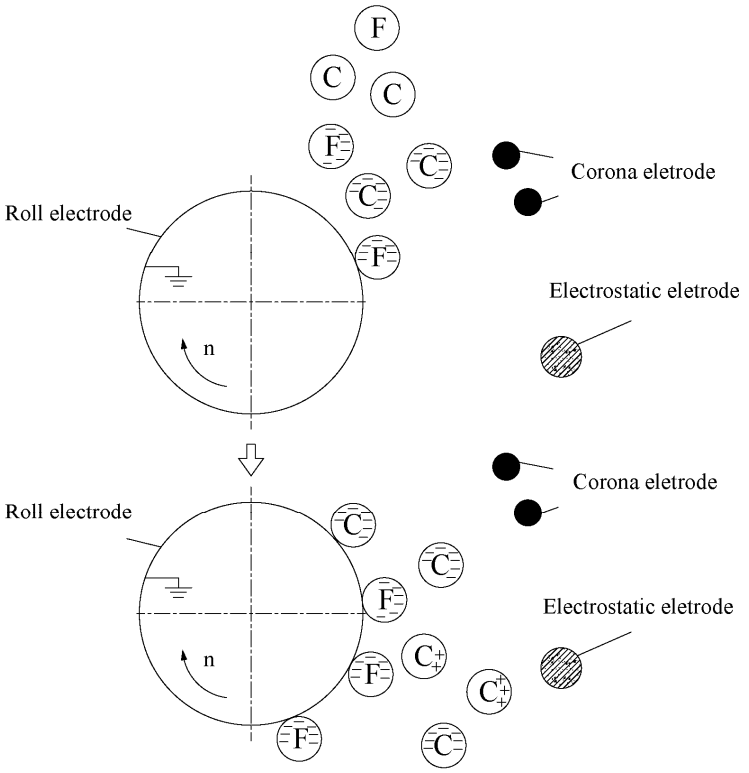


Figure 6. Model for the charging process. C: unginned cotton and F: residual film.

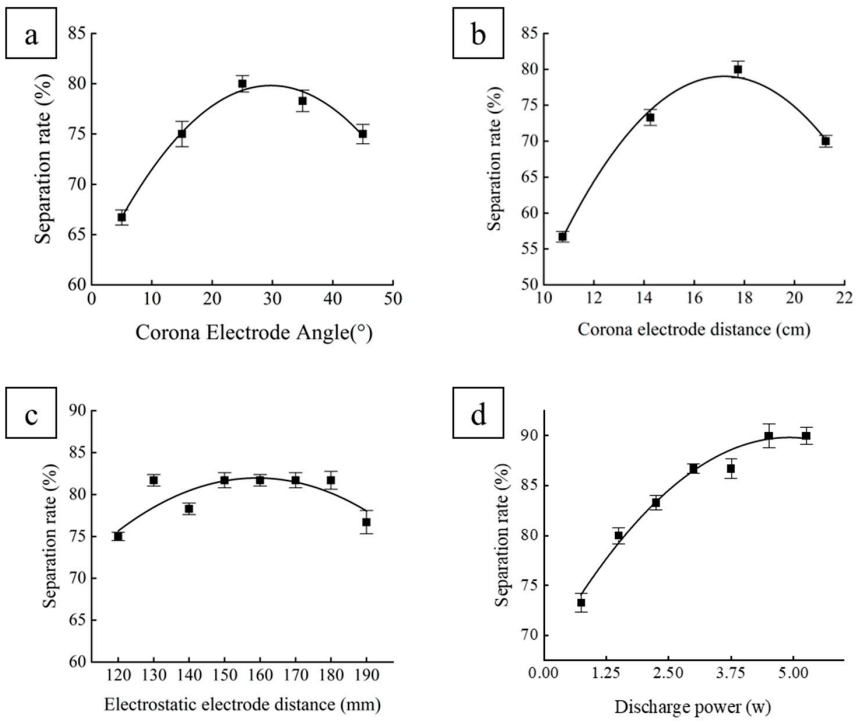


Figure 7. Relationships between the separation efficiency and the electrode position and other operating parameters. (**a**). Relationship between corona electrode angle and residual film separation rate, (**b**). Relationship between corona electrode distance and residual film separation rate, (**c**). Relationship between the electrostatic electrode position and the residual film separation rate, (**d**). Relationship between discharge power and separation rate.

With a discharge power of 1.5 W, a corona electrode angle of 20°, a θ_2 of 10°, and an S_2 of 180 mm, separation experiments were carried out with different corona electrode distances, and the separation rates were measured. The test results (Figure 7b) showed that when the distance between the electrical separation channels was less than 107.5 mm, the high-voltage electric field broke down the air to form an arc, resulting in a consumption of energy and a decrease in the separation rate. When the distance between the electrical separation channels was greater than 212.5 mm, the electric field intensity dropped sharply, and the residual film was not fully charged, leading to a greatly reduced separation rate. In fact, many materials passed through the space between the channels, and overly small separation distances led to an increased risk of material blockage. The test results showed that when the corona electrode distance was 142.5–212.5 mm, the residual film separation efficiency was the highest. A correlation analysis was carried out for corona electrode distances ranging from 107.5–212.5 mm.

With a discharge power of 1.5 W, a corona electrode angle of 20°, a distance of 177.5 mm, and a θ_2 of 10°, separation experiments were carried out with different electrostatic electrode distances S_2, and the separation rates were measured. The test results (Figure 7c) showed that when the electrostatic electrode was introduced, the electric field strength was increased [25], and the residual film separation rate increased significantly. The separation performance was better when the distances between the electrostatic electrodes were 130 mm and 160–180 mm. Correlation analyses were carried out for electrostatic electrode distances ranging from 120 to 190 mm.

With a corona electrode angle of 20°, a distance of 177.5 mm, a θ_2 of 10°, and an S_2 of 180 mm, separation experiments were carried out with different discharge powers, and the separation rates were measured. The test results (Figure 7d) showed that increased discharge power significantly increased the separation rate. The higher the discharge power was, the higher the separation rate. When the power exceeded 5.25 W, the separation rate did not increase. This is because the high field strength caused an intense ionic wind [31], which obstructed the entry of the residual film into the electric field and then affected the separation rate.

3.3.2. Response Surface Test for Electrostatic Separation of the Residual Film from the Unginned Cotton

The corona electrode angle A, corona electrode distance B, and discharge power C were selected as the independent variables, and the residual film separation rate Y was selected as the response value. The response surface method and Design-Expert software was used to design the response surface analysis scheme [32]. The analysis scheme and test results are shown in Table 3.

Table 3. Results of the response surface analysis.

Test No.	Corona Electrode Angle A/°	Corona Electrode Distance B/mm	Discharge Power C/w	Separation Rate Y/%
1	1	0	1	86.7
2	1	−1	0	80.0
3	−1	0	−1	83.3
4	1	1	0	66.7
5	0	1	1	83.3
6	0	−1	1	86.7
7	0	0	0	90.0
8	−1	1	0	83.3
9	−1	0	1	88.3
10	1	0	−1	73.3
11	0	0	0	86.7
12	−1	−1	0	73.3
13	0	0	0	86.7
14	0	−1	−1	70.0
15	0	0	0	93.3
16	0	0	0	86.7
17	0	1	−1	75.0

Multiple regression fitting was performed with the data in Table 3, and then a quadratic multiple regression equation based on A, B, C, and Y was obtained.

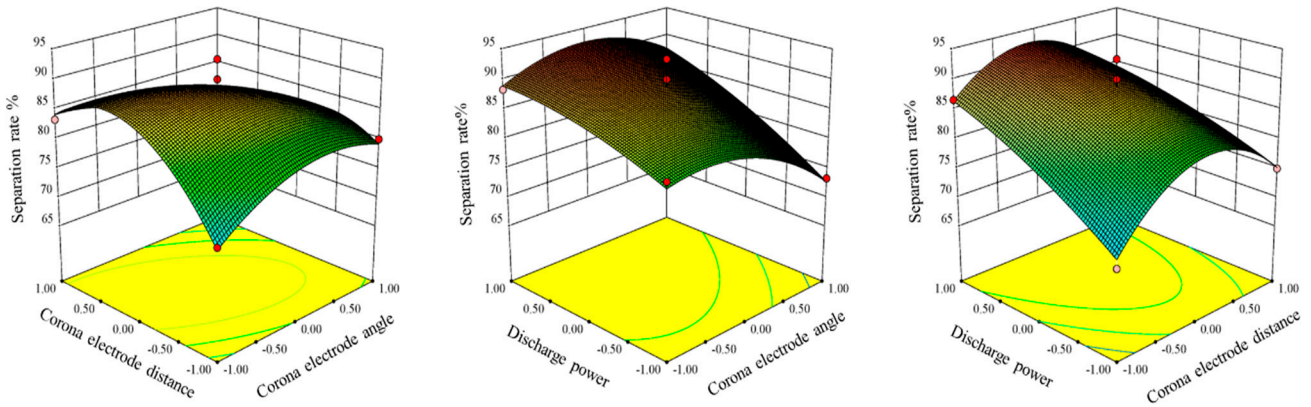
$$Y = 88.68 - 2.69A - 0.21B + 5.43C - 5.83AB + 2.10AC - 2.10BC - 4.35A^2 - 8.50B^2 - 1.43C^2$$

The analysis of variance (Table 4) showed that the p values were less than 0.01. This indicated that the model was highly significant. Since a p value greater than 0.05 indicates a lack of fit, the obtained regression equation is extremely significant. The coefficient of determination R^2 for the fitted quadratic regression equation was 0.9530, indicating a good fit. The equation correctly reflects the relationships between Y and A, B and C, and the model accurately predicts the test results.

Table 4. Analysis of variance for the effects of corona electrode angle, corona electrode distance, and discharge power on the residual film separation rate.

Sources	Sum of Squares	df	Mean Square	F Value	*p* Value
Model	885.69	9	98.41	15.78	0.0007
A	57.78	1	57.78	9.27	0.0187
B	0.36	1	0.36	0.058	0.8167
C	235.45	1	235.45	37.75	0.0005
AB	135.72	1	135.72	21.76	0.0023
AC	17.64	1	17.64	2.83	0.1365
BC	17.64	1	17.64	2.83	0.1365
A^2	79.77	1	79.77	12.79	0.009
B^2	304.39	1	304.39	48.81	0.0002
C^2	8.58	1	8.58	1.38	0.2792
Residual	43.66	7	6.24		
Lack of Fit	8.81	3	2.94	0.34	0.8009
Pure Error	34.85	4	8.71		
Cor Total	929.34	16			

According to the regression coefficients for each factor in the model, C had the greatest influence on Y, followed by A and B. To examine the relationships between the test indicators and factors, the influence of each factor was analyzed, and 3D response surface diagrams were drawn for the factor influences. The response surface diagrams for the effects of the corona electrode angle and the corona electrode distance on the separation rate are shown in Figure 8a. When the corona electrode angle was increased from 15° to 35°, the separation rate first increased and then decreased. When the corona electrode angle was kept at a certain level, as the corona electrode distance increased from 142.5 mm to 212.5 mm, the separation rate first increased and then decreased. The response surface diagram showing the effects of the corona electrode angle and the discharge power on the separation rate is provided in Figure 8b. When the corona electrode angle was increased from 15° to 35°, the separation rate first increased and then decreased. When the corona electrode angle was kept at a certain level, the separation rate generally increased as the discharge power was increased from 3.75 W to 5.25 W. The response surface diagram indicating the effects of the corona electrode distance and the discharge power on the separation rate is shown in Figure 8c. When the corona electrode distance was increased from 142.5 mm to 212.5 mm, the separation rate increased first and then decreased. When the corona electrode distance was kept at a certain level, the separation rate continued to rise with increasing discharge power.



(**a**) (**b**) (**c**)

Figure 8. Response surfaces showing the effects of each factor on the separation rate. (**a**) C = 4.5 w, (**b**) B = 172.5 mm, (**c**) A = 25°.

3.3.3. Determination and Verification of the Optimal Parameters

The maximum value of Y was used to optimize A, B, and C, and a model for the objective function of Y was established. Design-Expert software was used to optimize the parameters of the regression equation, and the optimal values for the three factors were obtained: the corona electrode angle was 25.3°, the corona electrode distance was 172.3 mm, and the discharge power was 5.25 W. For this combination, Y was 92.8%. The environmental temperature was 26°C, the humidity was 20–30%, and the moisture content of the unginned cotton was 3.5–4.9%. A verification test based on this combination of the optimized parameters was carried out and repeated six times. The separation rate was 91.7%, which was not very different from the results obtained with the optimal parameter combination. Therefore, the optimal parameter combination was consistent with the actual test results.

4. Conclusions

An electrostatic separation method was proposed for removing the residual film during cotton processing. Through theoretical analyses, the separation test platform was set up, the material charge tests were carried out, and finally, tests on the separation of seed cotton and the residual film were carried out. The results showed the following:

1. Based on the principles of corona charge and induction charge, a pin-roller electrostatic separation device was designed and used to separate the residual film in cotton during processing.
2. Corona electrodes were used to charge the materials, and electrostatic electrodes were used to form the electric fields. During operation, the electrostatic electrode repelled the negative residual film and attracted the positive unginned cotton, so the composite electrode structure with the corona electrode and the static electrode improved the separation efficiency.
3. The conductive properties of the unginned cotton and the residual film were investigated with material charge tests. The results showed that the unginned cotton with a moisture content of approximately 10% served as a conductor, so it contacted the electrode of the ground roller after charging and then carried a positive charge due to the influence of inductive charging. The residual film was a nonconductor, and the charge was not easily lost under the action of the electric image force, so the film continued to adsorb onto the ground roller electrode.
4. In the high-voltage electrostatic field of the corona discharge, the unginned cotton and residual film underwent quick and complete instantaneous charging during free fall through the ionization environment without deliberately increasing the charging

time of the material. For 12 random samples, the average charge on the residual films was −32.91 nC. The average charge of the unginned cotton that did not contact the ground electrode was −3.54 nC and that of the unginned cotton that did contact the ground electrode was 1.18 nC (positive value).

5. The results of the single factor tests showed that the optimal parameters for the separation of unginned cotton and residual film were in the following ranges; corona electrode angles of 15°–35°, corona electrode distances of 142.5 mm–212.5 mm, and discharge powers of 3.75 W–5.25 w.
6. The orthogonal test results show that the optimal parameter combination included a corona electrode angle of 25.3°, a corona electrode distance of 172.3 mm, and a discharge power of 5.25 W. In the optimization test, the separation rate reached 91.7%. These results showed that the needle roller-type electrostatic separation device met the design requirements for separating unginned cotton and residual films and the agronomic requirements for actual production.

Author Contributions: Methodology, Y.S. and R.Z.; software, Y.S. and C.H.; validation, R.Z. and C.H.; formal analysis, Y.L.; investigation, Y.S. and M.C.; data curation, Y.S.; writing—original draft preparation, Y.S.; writing—review and editing, R.Z. and C.H.; visualization, Y.S.; supervision, R.Z.; project administration, R.Z.; funding acquisition, R.Z. and C.H. All authors have read and agreed to the published version of the manuscript.

Funding: Science and Technology Research Plan in Key Fields of XPCC (2020AB006); Autonomous Region Key R&D Program (202004962); Shihezi University High-level Talents Research Startup Project (CJXZ202104).

Institutional Review Board Statement: Not applicable.

Data Availability Statement: The data presented in this study are available on demand from the first author at: (sunyue1@stu.shzu.edu.cn).

Acknowledgments: The authors would like to thank the technical support of the teacher and supervisor. We also appreciate the assistance provided by team members during the experiments. Moreover, we sincerely appreciate the work of the editor and the reviewers of the present paper.

Conflicts of Interest: The authors declare no conflict of interest.

References

1. Ren, W.; Du, Y.; Zuo, H. Research progress in image segmentation and edge detection methods for alien fibers detection in cotton. *J. Text. Res.* **2021**, *42*, 196–204. [CrossRef]
2. Wu, J.; Chen, X. Current situation, problems and countermeasures of cotton production mechanization development in Xinjiang Corps. *Chin. J. Agric. Eng.* **2015**, *31*, 5–10. [CrossRef]
3. Liang, R.; Chen, X.; Zhang, B. Current situation and countermeasures of the recovery methods and resource reuse of residual film in cotton fields in Xinjiang. *Chin. J. Agric. Eng.* **2019**, *35*, 1–13. [CrossRef]
4. Kan, Z.; Guo, W.; Zhang, R. Design of reticulated drum machine-unginned cotton residual membrane separator. *Chin. J. Agric. Eng.* **2011**, *27*, 95–99. [CrossRef]
5. Li, H.; Wang, H. Multi-objective adaptive control model of foreign fiber cleaner used in seed cotton. *Chin. J. Agric. Eng.* **2015**, *31*, 39–46. [CrossRef]
6. Liu, X.; Zhou, Y.; Zhao, Y. The current situation and prospect of the development of cotton foreign fiber cleaning machinery. *Jiangsu Agric. Sci.* **2011**, *39*, 505–506. [CrossRef]
7. Peng, Q.; Li, C.; Kang, J. Improved design and experiment of pneumatic cylindrical sieve membrane hybrid separator. *J. Agric. Mach.* **2020**, *51*, 126–135. [CrossRef]
8. Ni, C.; Li, Z.; Zhang, X. Unginned cotton mulch sorting algorithm based on short-wave near-infrared hyperspectral and deep learning. *J. Agric. Mach.* **2019**, *50*, 170–179. [CrossRef]
9. Yu, J.; Li, C. mRMR-based feature selection for classification of cotton foreign matter using hyperspectral imaging. *Comput. Electron. Agric.* **2015**, *119*, 191–200. [CrossRef]
10. Kuzy, J.; Li, C. A pulsed thermographic imaging system for detection and identification of cotton foreign matter. *Sensors* **2017**, *17*, 518. [CrossRef]
11. Zhang, M.; Li, C.; Yang, F. Classification of foreign matter embedded inside cotton lint using short wave infrared (SWIR) hyperspectral transmittance imaging. *Comput. Electron. Agric.* **2017**, *139*, 75–90. [CrossRef]

12. De Oliveira, C.M.; Bellopede, R.; Tori, A.; Zanetti, G.; Marini, P. Gravity and Electrostatic Separation for Recovering Metals from Obsolete Printed Circuit Board. *Materials* **2022**, *15*, 1874. [CrossRef]
13. Suponik, T.; Franke, D.M.; Nuckowski, P.M.; Matusiak, P.; Tora, B. Impact of grinding of printed circuit boards on the efficiency of metal recovery by means of electrostatic separation. *Minerals* **2021**, *11*, 281. [CrossRef]
14. Zhang, Z.; Cui, Z.; Yang, J.; Yue, Z.; Wei, Y. Optimization of electrostatic separation of Si and PET in waste solar panels. *China Environ. Sci.* **2017**, *37*, 3048–3055. [CrossRef]
15. Salama, A.; Richard, G.; Medles, K.; Zeghloul, T.; Dascalescu, L. Distinct recovery of copper and aluminum from waste electric wires using a roll-type electrostatic separator. *Waste Manag.* **2018**, *76*, 207–216. [CrossRef]
16. Xu, A.; Niu, X.; Hu, Y.; Yang, Y. Study on adsorption efficiency of electrostatic residual membrane separation device. *Jiangsu Agric. Sci.* **2017**, *45*, 204–207. [CrossRef]
17. Xu, A.; Ma, S.; Hu, Y.; Niu, X. Effects of moisture content and voltage on the efficiency of electrostatic separation devices. *Res. Agric. Mech.* **2017**, *45*, 204–207. [CrossRef]
18. Qi, Y.; Yang, Y.; Wang, Y. Residual membrane electrostatic adsorption experimental study on the recovery unit. *J. Agric. Mech. Res.* **2021**, *43*, 164–168. [CrossRef]
19. Guo, S.; Kan, Z.; Zhang, R.; Guo, W. Separation test of electrostatic separation device for mechanically harvested unginned cotton residual film. *Chin. J. Agric. Eng.* **2011**, *27*, 6–10. [CrossRef]
20. Wang, Q.; Weng, F.; Zhang, H.; Yuan, C.; Li, L. Grading removal of residual plastic film in machine-harvested cotton using electrostatic adsorption method. *Trans. Chin. Soc. Agric. Mach.* **2019**, *50*, 140–147.
21. Labair, H.; Touhami, S.; Tilmatine, A.; Hadjeri, S.; Medles, K.; Dascalescu, L. Study of charged particles trajectories in free-fall electrostatic separators. *J. Electrost.* **2017**, *88*, 10–14. [CrossRef]
22. Xue, M.; Yan, G.; Li, J.; Xu, Z. Electrostatic separation for recycling conductors, semiconductors, and nonconductors from electronic waste. *Environ. Sci. Technol.* **2012**, *46*, 10556–10563. [CrossRef]
23. Li, M.; Hu, W.; Gong, W. Influence of electrode structure on the electric field of YD electro-separator. *Min. Metall. Eng.* **2016**, *36*, 30–32.
24. Peng, Z.; Yang, X.; Wang, H.; Zhang, G.; Yang, J.; Zhao, X. Research on friction electrostatic separation of ilmenite. *Met. Mines* **2018**, *02*, 80–84. [CrossRef]
25. Richard, G.; Salama, A.; Medles, K.; Zeghloul, T.; Dascalescu, L. Comparative study of three high-voltage electrode configurations for the electrostatic separation of aluminum, copper and PVC from granular WEEE. *J. Electrost.* **2017**, *88*, 29–34. [CrossRef]
26. Chen, Z.; Xia, Q.; Huang, Q. Study on electrical properties of wheat bran structure layer powder. *Chin. J. Agric. Eng.* **2020**, *36*, 303–309. [CrossRef]
27. Jafari, M.; Chegini, G.; Akmal, A.A.S.; Rezaeealam, B. A roll-type corona discharge–electrostatic separator for separating wheat grain and straw particles. *J. Food Process Eng.* **2019**, *42*, e13281. [CrossRef]
28. Zhang, X.; Su, Y.; Yi, J. Experimental study on the effect of rubbing pretreatment on shelling of Penaeus vannamei. *Chin. J. Agric. Eng.* **2021**, *37*, 307–315. [CrossRef]
29. Yang, S.; Chen, X.; Yan, L. Design and experiment of a belt-type film reel device for residual film recovery machine. *J. Agric. Mach.* **2021**, *52*, 135–144. [CrossRef]
30. Li, F.; Xing, S.; Tian, F. Design and experiment of tooth roller type forage crop preparation test bench. *J. Agric. Mach.* **2021**, *52*, 136–147. [CrossRef]
31. Li, Q.; Liu, X.; Ju, X. Influencing factors of ion distribution under needle-plate electrode negative corona discharge. *High Volt* **2017**, *43*, 1700–1706. [CrossRef]
32. Ge, Y. *Experimental Design Method and Application of Design-Expert Software*; Harbin Institute of Technology Press: Harbin, China, 2015; pp. 62–95.

Disclaimer/Publisher's Note: The statements, opinions and data contained in all publications are solely those of the individual author(s) and contributor(s) and not of MDPI and/or the editor(s). MDPI and/or the editor(s) disclaim responsibility for any injury to people or property resulting from any ideas, methods, instructions or products referred to in the content.